Experiments and Analysis of High Cyclic Variability at the Operational Limits of Spark-Assisted HCCI Combustion

Jacob Larimore, Erik Hellström, Jeff Sterniak, Li Jiang, Anna G. Stefanopoulou

***Abstract*— During combustion mode switches, between homogeneous charge compression ignition (HCCI) and spark ignition (SI) combustion, the engine will operate at throttled and stoichiometric conditions where high cyclic variability (CV) is typically observed. To analyze and eventually model the engine behavior at the high CV condition we perform measurements on a four-cylinder HCCI engine with negative valve overlap and describe a cycle-resolved analysis method that enables the characterization of cycle-to-cycle variations at such conditions.**

The dynamic behavior observed is characterized by the recycling of thermal and chemical energy between cycles. We quantify the cyclic exchange and relate it to the dynamic patterns that emerge from this high CV condition. We also clarify the contributions of the spark at these conditions, where advancing the spark can significantly reduce the variability. It is our conclusion that the dynamic patterns observed can be characterized by the cycle-resolved combustion efficiency as it is an essential non-linearity in the dynamic evolution.

I. Introduction

Homogeneous charge compression ignition (HCCI) combustion with negative valve overlap (NVO) is a re-compression strategy used to achieve HCCI combustion in which the charge temperature is raised by closing the exhaust valve early, trapping hot residual gases [1]. HCCI combustion has the advantage of being very efficient while producing low amounts of emissions. A drawback is, however, a limited operating range compared to conventional spark ignited (SI) combustion. A way of extending the operating range is to switch between combustion modes as demonstrated in [2].

Performing a fast mode switch with a smooth torque output is a challenging task due to the many actuators that require coordination and the high combustion variability in a transition as shown in [3]. For example, a smooth transition from HCCI, with lean mixture, to SI, with stoichiometric mixture, requires maintaining torque with low variability while reducing the air-fuel ratio. The dynamics in the air path are slower than the combustion process and it is therefore desirable to, in a transient, operate HCCI combustion throttled and closer to stoichiometry than in the normal operating range. Moreover, the reduction in air mass when closing the throttle can be counteracted by reducing the NVO. Reduction of the residual gas fraction lowers the temperature at intake valve closing and retards the combustion phasing. At late phasing the variability can increase significantly as shown in [4], [5].

The variability of HCCI combustion has been studied in [6] in simulation and it was shown that there is a strong coupling of consecutive cycles due to recycled thermal energy. The important addition of the effects of recycled chemical energy were introduced through simulations of chemical kinetics with 31 species in [7] and reduced to an eight state model in [8]. A control oriented, 4 state, model was developed in [9] where fuel was one of the states. Experiments for lean HCCI were studied and modeled with two states in [4], [5]. While the stoichiometric case has been observed in the transition from SI to HCCI in [3], [10], [11]. It will be shown that the dynamic coupling appears to be different for lean versus stoichiometric HCCI. The unburned fuel mass that couples the cycle-to-cycle behavior is quantified here and sheds light on the chemical energy coupling and the dynamical patterns emerging at the limits of the HCCI stability region. Extending the gross heat release analysis performed at the limits of lean HCCI in [4], [5] we observe a distinct pattern in combustion efficiency versus phasing. This efficiency correlation provides a key non-linear characteristic that distinguishes cyclic variability at the lean versus the stoichiometric spark-assisted limit, [12]. Additionally it yields insights as to the contribution of spark.

Our aim is to improve the understanding of the complex behavior of throttled stoichiometric HCCI combustion. To this end we use cylinder pressure data and an analysis method suitable for cycle resolved study of combustion with high variability. Similar to [5], we complement the iterative method with an estimate for residual gas fraction derived from [13] modified to accommodate high combustion variability. A study of this method in [14] shows that among other approaches, the Mirsky method of [15] and the state equation method derived from [16], that this basis is the most robust. However it is also noted that it needs improvements in some operating regions. This work aims to resolve some of these inaccuracies. Other methods derived for SI combustion have been considered and can be found in [17], [18].

The paper is organized as follows. First the experimental setup is described. Next, the methods used to analyze the raw data are detailed. After that, observations on the CV are made and finally, conclusions about the behavior are presented.

II. Experimental Setup

The experiments were performed on a 4 cylinder 2 L GM Ecotec engine running on EPA Tier II EEE certification fuel. The engine is installed and operated in the Automotive Laboratory at the University of Michigan. Modifications of the engine for HCCI combustion include increasing the compression ratio to 11.25 and using a camshaft with a lower lift and shorter duration valve profile suitable for HCCI operation with NVO. In addition a Borg-Warner KP31

J. Larimore (larimore@umich.edu), E. Hellström (erikhe@umich.edu) and A. Stefanopoulou (annastef@umich.edu) are with the Department of Mechanical Engineering in the University of Michigan, Ann Arbor. J. Sterniak (jeff.sterniak@us.bosch.com) and L. Jiang (li.jiang@us.bosch.com) are with Robert Bosch LLC, Farmington Hills.

turbo provides boost. Cylinder pressure was sampled with a resolution of 0.1 cad and, in order to thoroughly observe the cycle dynamics, 3000 consecutive cycles were obtained. The test was run at 2000 rpm, regulated by a DC dynamometer, and fuel was maintained constant to give approximately 4 bar net indicated mean effective pressure (IMEP). Engine coolant temperature was maintained constant throughout the test and spark was fixed at top dead center for main combustion (TDCm), between IVC and EVO. Fuel injection was at 60° after TDCn, defined as between EVC and IVO.

To explore the limits of operation, the throttle angle was gradually reduced while maintaining stoichiometry, as indicated by the exhaust lambda sensor, by compensating through reduced NVO. When the variability, in terms of coefficient of variation (CoV) of IMEP, passed the acceptable limit of 5% all actuators were held constant and the measurements were recorded. The engine was thus run in open-loop except for control of engine speed and coolant as described above. This level of CoV corresponded to 25% throttle and an NVO of 144°, the result of which is a residual gas fraction of approximately 44%. Boost pressure before the throttle was 1.39 bar while the intake and exhaust manifold pressure were at 1.05 and 1.44 bar, respectively.

III. Analysis Method

An analysis method is presented for the determination of cylinder temperature, heat release, unburned fuel, combustion efficiency and residual gas fraction. The method is iterative and derived from mass and energy balances. A flow diagram of the process is shown in Fig. 1. A basis of this method is presented in detail by [5], [13] however a summary with modifications is presented here to allow for extension to abnormal cycles and boosted conditions.

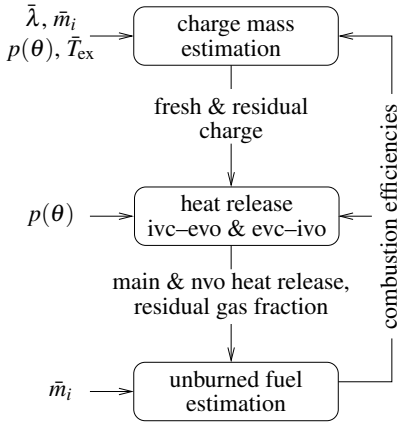

Fig. 1. Block Diagram for the estimation routine.

A. Charge Mass Estimation

Crucial to combustion analysis in HCCI is the determination of the mass of residuals carried from one cycle to the next. This can be defined as the mass of charge at EVC as given by the ideal gas law, $m_{res} = P_{evc}V_{evc}/RT_{evc}$, where m_{res} is the mass of residuals. The in cylinder pressure is measured and the volume, V, is known. The gas constant, R, is for burned gas composition and is constant. Therefore to determine m_{res} we must find T_{evc}. To do so we develop a system of equations, from which T_{evc} may be solved.

We assumes steady state conditions for the air path and so the mass of fresh air and fuel inducted into the cylinder is equal to the mass that leaves through the exhaust process,

$$m_{out} = \frac{P_{evo}V_{evo}}{RT_{evo}} - \frac{P_{evc}V_{evc}}{RT_{evc}} = m_{air} + m_{fuel} \quad (1)$$

where the pressures at the valve events are measured, as is the mass of fresh air, m_{air}, and the mass of injected fuel, m_{fuel}. This gives one equation with two unknowns, T_{evo} & T_{evc}, therefore additional relations are needed.

By assuming the exhaust process is reversible, the differential heat loss per unit mass can be described by

$$\delta q = Tds = c_p dT - \frac{RT}{P}dP \quad (2)$$

where c_p is the specific heat and is assumed constant. Splitting the exhaust process into two parts and integrating yields

$$q_1 = \int_{T_{evo}}^{T_{ref}} c_p dT - R\int_{P_{evo}}^{P_{ref}} \frac{T}{P}dP \quad (3)$$

$$q_2 = \int_{T_{ref}}^{T_{evc}} c_p dT - R\int_{P_{ref}}^{P_{evc}} \frac{T}{P}dP \quad (4)$$

$$r_{ex} \equiv q_1/q_2 \quad (5)$$

the ratio of which is defined by Eq. (5) and will be called the heat transfer ratio, r_{ex}. The point used to split the exhaust process in two, defining the integration limits, will be referred to as the reference point. In [13] it is taken as the point at which the exhaust runner pressure is equal to 1 atm. To ascertain that there always is a reference point, even for boosted conditions, one could instead use the point of minimum pressure as in [5]. However, if the minimum occurs close to valve events the ratio is close to zero or infinity which may give rise to numerical issues. For example, it was observed that the minimum may be at EVO following a misfire. Therefore, the reference point is here chosen to be fixed at the middle of the valve open period.

The variable T_{ref} is the exhaust gas temperature at the reference point. This is taken to be the measured exhaust runner temperature while P_{ref} is the measured cylinder pressure at the reference point. It is recognized that there may be a difference between the measured and actual temperature of the gas, due to cooling of the thermocouple during the valve closed periods of the cycle, however analysis in [19], [20] has shown that an offset of ± 50 K has an approximate 2% effect on the resulting residual gas fraction. Based on this we approximate the measured value as the actual gas temperature.

The heat transfer ratio, Eq. (5), is an additional unknown however it can be approximated using the model

$$q_i = \int_i h_c A(T_{cyl} - T_w)dt, \quad i = 1, 2. \quad (6)$$

The heat transfer coefficient is determined using the Woschni method as in [16] and a constant wall temperature is

assumed. The time–varying temperature T_{cyl} is determined from T_{evo}, T_{evc} and T_{ref} assuming a polytropic process. Equations (1), (5) and (6) are three nonlinear equations for the unkowns (r_{ex}, T_{evo}, T_{evc}), which are solved with the following iterative approach. For a given r_{ex} Eqs. (1) and (5) yield an analytically solved quadratic in T_{evo} and T_{evc}. Inserting the (pysically reasonable) solution into Eq. (6) gives a new value for r_{ex}. This fixed-point iteration is continued until convergence. This method never required more than three iterations for the data analyzed and is therefore a fast and efficient way of solving the sytem of equations. The initial guess for r_{ex} is 1, based on the reasonable assumption that the heat transfer in the two parts of the exhaust process are nearly equal. With the solution (r_{ex}, T_{evo}, T_{evc}), the mass of residuals may be found with the ideal gas law. The residual gas fraction is then determined by $x_r = m_{res}/(m_{air} + m_{fuel} + m_{res})$.

B. Gross Heat Release

Gross heat release is found for both main combustion and NVO using the first law of thermodynamics $Q(\theta) = Q_{net}(\theta)+Q_{ht}(\theta)$ as defined by Eqs. (7) (8) which are the heat release due to combustion and heat transfer respectively. The heat transfer coefficient was determined using the modified Woschni correlation presented in [21] and a constant wall temperature was assumed.

$$\frac{dQ_{net}}{d\theta} = \frac{1}{\gamma - 1} VdP + \frac{\gamma}{\gamma - 1} PdV \tag{7}$$

$$\frac{dQ_{ht}}{dt} = Ah_c(T_{cyl} - T_w) \tag{8}$$

The value of γ is calculated on a crank angle basis as determined by the composition of the mixture, $\xi(\theta) = (1 - x_b(\theta))\xi_u + x_b(\theta)\xi_b(\theta)$, and by the mass fraction burned $x_b(\theta) = \eta Q(\theta)/\max Q(\theta)$, where $\xi_b(\theta)$ and $\xi_u(\theta)$ are the composition of the burned and unburned mixtures, respectively, and $\xi_b(\theta)$ is computed for chemical equilibrium at $P(\theta)$ and $T(\theta)$.

C. Unburned Fuel Estimation

Data with high variability can have cycles with incomplete burns. When this occurs a portion of the fuel is left unburned and carried over to the next cycle, through NVO. This residual fuel has a major impact on behavior of the engine and it is therefore important to quantify it. To do so the mass of unburned fuel is computed from the difference equation derived in [5],

$$m_u(k+1) = x_r(k)\left(\bar{m}_i + m_u(k) - \tfrac{Q_m(k)}{q_{lhv}}\right) - \tfrac{Q_n(k)}{q_{lhv}}, \tag{9}$$

which is dependent on an initial unburned fuel mass, $m_u(0)$. Here $Q_m(k)$ is the maximum value of the heat release between IVC and EVO while $Q_n(k)$ is the maximum between EVC and IVO, q_{lhv} is the lower heating value of the fuel and $\bar{m}_i$ is the average mass of injected fuel. An analysis of this equation in [22] shows that it will converge to the correct value given any initial guess within a small number of iterations. Here the amount of unburned fuel is assumed to be zero initially and convergence was achieved in less than 8 cycles. Finally the combustion efficiencies are found from

$$\eta_m(k) = \frac{Q_m(k)/q_{lhv}}{m_f(k)}, \tag{10}$$

$$\eta_n(k) = \frac{Q_n(k)/q_{lhv}}{x_r(k)(m_f(k) - Q_m(k)/q_{lhv})} \tag{11}$$

where $\eta_m(k)$ and $\eta_n(k)$ are for main and NVO, respectively. The mass of fuel is defined as $m_f(k) = \bar{m}_i + m_u(k)$. These efficiencies are used in the next iteration of heat release and x_r as described by Fig. 1, iterations continue until the change in both efficiencies is sufficiently small.

IV. Discussion of Results

The measurements from the experiments and the results from the analysis method in Sec. III are discussed. The observations collectively show that unburned fuel carries over to the NVO period and to the next cycle. The effects are heat release during NVO and higher than normal heat release during main combustion. The analysis method quantifies these effects by estimating the unburned fuel amount and the combustion efficiencies. The pressure data for 3000 cycles

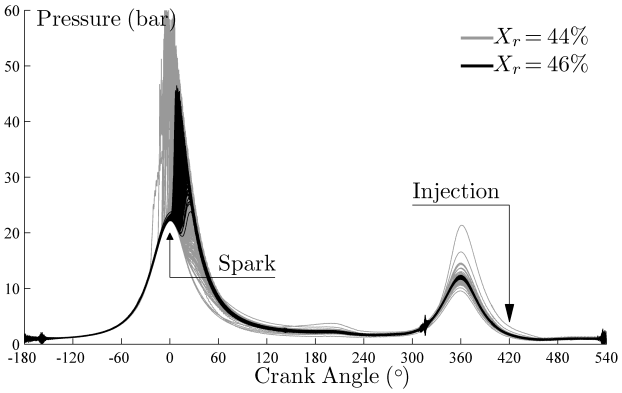

Fig. 2. Raw pressure data. The large difference in variation from cycles in black to those in gray is due to a small change in x_r.

in two operating points is shown in Fig. 2. The operating conditions in Fig. 2 are different with respect to x_r. This difference arises from a change in throttle and NVO. The points in black are throttled to 30% while gray are at 25%, as the throttle percentage is increased the NVO also increases to maintain stoichiometry and as a result x_r is raised. Cycles in black have a slightly higher x_r than those in gray and are considered normal burns. As can be seen in Fig. 2 when x_r is lowered slightly the data becomes highly variable. In addition, for some cycles in gray, a significant pressure rise during NVO can be observed. The cycles in gray will be the focus of this work.

In conjunction, Fig. 3 shows the gross heat release and cylinder temperatures for the two different levels of x_r. It can be seen that cycles which have low burns during main combustion tend to have a noticeable heat release during NVO. The corresponding temperatures are also high.

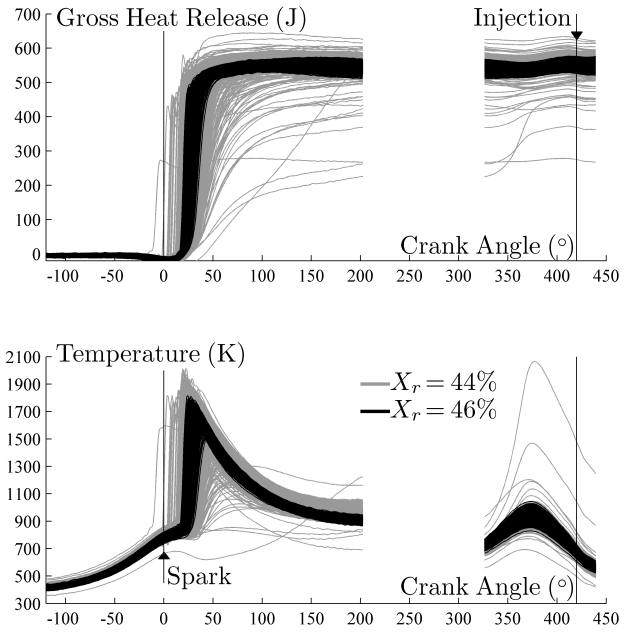

Fig. 3. Variation in heat release (top) and temperature (bottom) due to a small change in x_r.

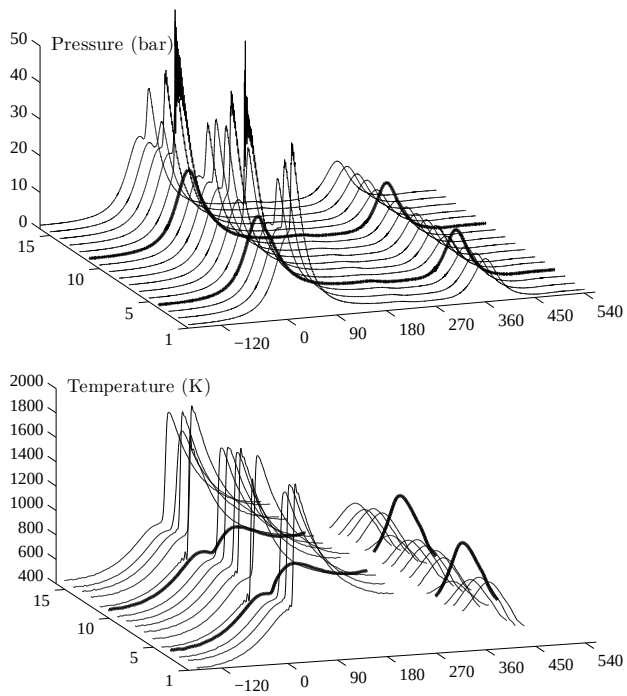

Fig. 4. Pressure and temperature for a sequence of cycles.

A. Cycle-to-cycle dynamics

To understand the cycle-to-cycle behavior further 16 cycles are observed in detail through an illustrative progression in Figs. 4–8. First, Fig. 4 shows both the evolution of cylinder pressure and temperature. The cycles highlighted in black, corresponding to cycles 4 and 11, are points with low heat release. Leading up to these cycles the peak pressures drop as do the temperatures. Consequently, cycles 4 and 11 exhibit a large temperature and pressure rise during the NVO period. It will be shown that this is result of unburned fuel. These cycles can be observed in Fig. 5 through a plot of combustion phasing versus efficiency. Cycles 1–3 maintain a relatively constant efficiency while phasing retards. This is followed by a rapid decline in efficiency in cycle 4 and then a moderately low efficiency in cycle 5 which has a 50% burn angle before TDC. The system then exhibits a very large burn and high efficiency at cycle 6 and returns to normal combustion in cycle 7. The rest of the cycles in this series are shown in light gray. An operating point with the same actuator settings, but with spark at 25° aTDC, is in dark gray.

It should be noted that cycles with low efficiencies on the left hand side of Fig. 5 are preceded by the cycles with the latest combustion phasing on the right hand side of the return map in Fig. 8. This shows that the heat release during NVO is affecting the temperature and pressure at IVC in cycle (k+1). Additionally it is possible that heat transfer is higher at these early phasings due to high ringing and turbulence. As a result these cycles may have a slightly higher efficiency than indicated in Fig. 5 due to underepresented heat losses in the analysis. However, the last cycle in these sequences, see cycle 6 and 13 in Fig. 6, has a higher than average heat release indicating unburned fuel from previous cycles.

When phasing is later the efficiency curve once again drops. This is explored in detail in [23], [24] where lean HCCI without the presence of spark is the topic of interest. However, when a comparison of the efficiencies is made between that of [24] and Fig. 5 one can notice that the spark improves the combustion efficiency of the cycles with late phasing by making their burns more complete. Figure 5 further demonstrates this for stoichiometric conditions. When the spark is advanced, as represented by the data in dark gray, there is a smaller variability and the peak efficiency is lower than that of the data with spark at TDC, shown in light gray. The progression of events is more clearly revealed

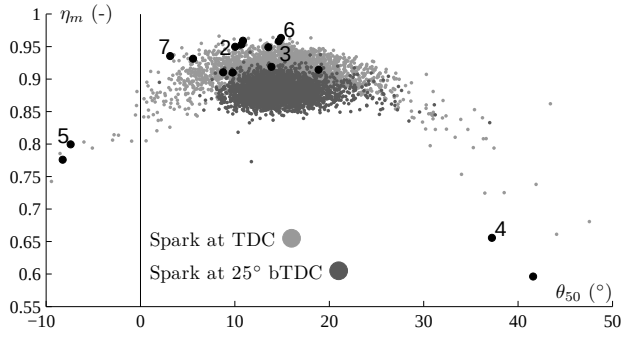

Fig. 5. Estimated efficiency for main combustion for operation with spark at TDC and 25° bTDC. The marked cycles corresponding with the cycles of Fig. 4–7.

in the consecutive heat releases of Fig. 6 and the trends of combustion phasing, IMEP and unburned fuel in Fig. 7. It should be noted that the amount of unburned fuel in Fig. 7 is the amount of extra fuel present at the beginning of each

cycle. Here we see that cycles 1–3 maintain a relatively constant IMEP however combustion phasing gradually shifts later until cycle 4 which is so late that the burn is very slow and little heat is released. This is most likely caused by the spark igniting the mixture rather than pure auto-ignition. Because cycle 4 is so poor a significant portion of the fuel is left unburned through main and NVO heat release, it is then carried over to cycle 5. This extra fuel accompanied by a high temperature at IVC, caused by the heat release during NVO of the previous cycle (4), results in a very rapid, and early, auto-ignition with a low combustion efficiency as indicated by Fig. 5 and a high ringing index as can be seen by the very large pressure spike, followed by oscillations, in Fig. 4. In addition, cycle 5's combustion appears to stop and is followed by a slow burn, initiated after the spark at TDC. Because of the low efficiency of this burn even more fuel is left unburned, as seen in Fig. 7, and carried over to the next cycle (6). However, cycle 5's conditions were not sufficient for NVO heat release, in fact there was very little temperature rise during NVO as seen in Fig. 4. As a result, cycle 6 once again behaves like normal HCCI combustion, however the build up of unburned fuel from the previous two cycles causes it to have a higher than normal heat release. Finally the system returns to HCCI combustion with the expected release of energy in cycle 7. Cycles 8 through 16 exhibit a similar sequence of events.

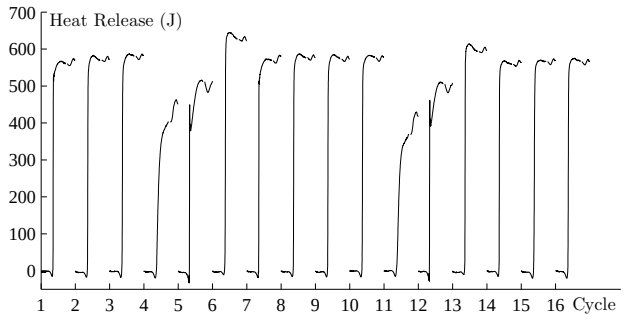

Fig. 6. Progression of abnormal cycles as seen by the variation in consecutive heat release during main and NVO.

B. Return Maps

To understand the cycle-to-cycle dynamics, return maps are presented. Such maps show the relationships between consecutive cycles and give insights about the dynamical coupling between cycles [25]. For example, in combustion with low variability the combustion phasing θ_{50} in cycle k and $k+1$ do not differ significantly from each other, the value of θ_{50} always returns to a similar value, and the points in the return map remain close to the diagonal. Figure 8 contains the return maps of heat transfer and combustion phasing as determined from the data analysis. Clear patterns emerge in the form of legs indicating a deterministic coupling between cycles. The vertical legs here correspond to an instability; they show that an average value for cycle (k) can result in an abnormal value in cycle (k+1). For example, if a cycle has a low heat release, a series of cycles which follow the

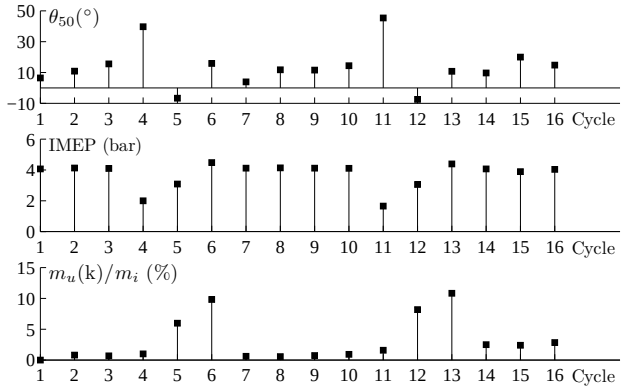

Fig. 7. Progression of abnormal cycles in terms of combustion phasing (top), IMEP (middle) and residual fuel (bottom).

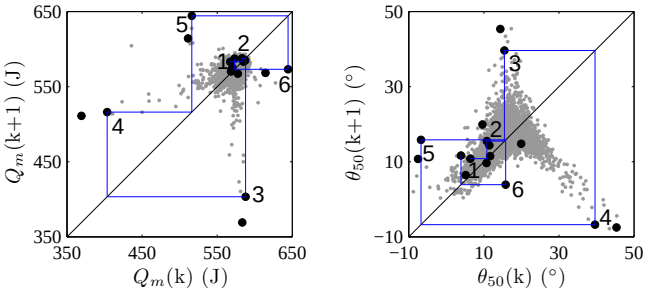

Fig. 8. Return maps of heat release (left) and combustion phasing (right). Consecutive cycles shown correspond to those of Fig. 7

dynamic behavior described by the orientation of the legs in the return maps is the result. Since the engine is operating close to the stability limit small perturbations in the system can cause such a scenario to occur.

Figure 8 shows the cycles as they progress through the return map legs. One can see in the map of combustion phasing that as we move from 1–2–3 the phasing walks up the diagonal becoming later and later. However, when following these same cycles in Fig. 5 we see that the efficiency remains at nearly the same level. As this phasing becomes later the charge temperature at IVC drops, causing the onset of instabilities. The third cycles' late phasing and high efficiency lead to cycle 4 which is extremely retarded and with very little heat released. The following cycles are a recovery from this poor burn. It is this series of cycles which defines the deterministic shapes of the return maps.

The heat release patterns that emerge from Fig. 8 share many resemblances with those presented in [3], [10], [11] where a single cylinder engine was used. These experiments were also run at stoichiometry and with NVO. Despite a change in the engine platform, the deterministic patterns are similar. However, when a comparison is made with results for lean operation in [4], [5] one can see that the shapes do not resemble those of Fig. 8 indicating a different non-linear behavior for lean versus stoichiometric HCCI.

V. Conclusions

Experimental data and a method for processing high CV spark-assisted HCCI combustion are presented. An extension for estimation of x_r on a per cycle basis, with high CV, is provided to compliment standard methods. These data analysis tools were applied to both main and NVO combustion and yielded important information to understand of the cyclic behavior observed, they can be summarized by the following:

- The results have been described using unburned fuel and combustion efficiency. This indicates that a control oriented model which captures the recycled thermal and chemical energy may be sufficient to describe the process. In addition, combustion efficiency is a way to capture the lumped effect of complex combustion chemistry.
- Unburned fuel carries over from cycle to cycle and can build up over a sequence of cycles before a large heat release occurs. This differs from lean operation where unburned fuel does not build up over a series of cycles.
- The patterns that emerge from this multi-cylinder engine resemble those of a single cylinder indicating that the most dominating mechanisms are similar regardless of engine platform or manifold filling dynamics.

The fuel that is carried over also leads to some heat release during the NVO period which can affect charge temperature on the next cycle. Therefore, a strong cycle-to-cycle coupling is present from fuel and temperature and they affect combustion efficiency directly. The observation, and quantification of this coupling is vital to understanding the dynamics of the cyclic variability which will help in the prediction and control of a smooth switch from HCCI to SI.

Acknowledgments

For valuable help in the set up and maintenance of the engine test cell, we thank Dr. Stani Bohac and Adam Vaughan at the University of Michigan. This material is supported by the Department of Energy [National Energy Technology Laboratory] DE-EE0003533[1] as a part of the ACCESS project consortium under the direction of the PI Hakan Yilmaz, Robert Bosch, LLC.

References

[1] J. Willand, R.G. Nieberding, G. Vent, and C. Enderle. The knocking syndrom – its cure and its potential. *SAE Tech. Papers*, 982483, 1998.

[2] L. Koopmans, H. Ström, S. Lundgren, O. Backlund, and I. Denbratt. Demonstrating a SI-HCCI-SI mode change on a Volvo 5-cylinder electronic valve control engine. In *SAE World Congress*, 2003. SAE 2003-01-0753.

[3] C. S. Daw, R. M. Wagner, K. D. Edwards, and J. B. Green Jr. Understanding the transition between conventional spark-ignited combustion and HCCI in a gasoline engine. *Proc. of the Comb. Inst.*, 31(2):2887–2894, 2007.

[1] Disclaimer: This report was prepared as an account of work sponsored by an agency of the United States Government. Neither the United States Government nor any agency thereof, nor any of their employees, makes any warranty, express or implied, or assumes any legal liability or responsibility for the accuracy, completeness, or usefulness of any information, apparatus, product, or process disclosed, or represents that its use would not infringe privately owned rights. Reference herein to any specific commercial product, process, or service by trade name, trademark, manufacturer, or otherwise does not necessarily constitute or imply its endorsement, recommendation, or favoring by the United States Government or any agency thereof. The views and opinions of authors expressed herein do not necessarily state or reflect those of the United States Government or any agency thereof.

[4] E. Hellström and A.G. Stefanopoulou. Modeling cyclic dispersion in autoignition combustion. In *Proc. 50th IEEE Conference on Decision and Control*, pages 6834–6839, 2011.

[5] E. Hellström, A. G. Stefanopoulou, J. Vávra, A. Babajimopoulos, D. Assanis, L. Jiang, and H. Yilmaz. Understanding the dynamic evolution of cyclic variability at the operating limits of HCCI engines with negative valve overlap. In *SAE World Congress*, 2012. SAE 2012-01-1106.

[6] C.J. Chiang and A. G. Stefanopoulou. Stability analysis in homogeneous charge compression ignition (HCCI) engines with high dilution. *IEEE Trans. on Control Sys. Tech.*, 15(2):209–219, March 2007.

[7] K.L. Knierim, S. Park, J. Ahmed, A. Kojic, I. Orlandini, and A. Kulzer. Simulation of Misfire and Strategies for Misfire Recovery of Gasoline HCCI. *2008 American Control Conference*, pages 3947–3952, 2008.

[8] C.G. Mayhew, K.L. Knierim, N.A. Chaturvedi, S. Park, J. Ahmen, and A. Kojic. Reduced-order Modeling for Studying and Controlling Misfire in Four-Stroke HCCI Engines. *Proc. of the 48th IEEE Conference on Decision and Control*, pages 5194–5199, 2009.

[9] N. Ravi, H.H. Liao, A.F. Jungkunz, and J.C. Gerdes. Modeling and control of exhaust recompression HCCI using split injection. *2010 American Control Conference*, 2010.

[10] C.S. Daw, K.D. Edwards, R.M. Wagner, and Jr. J.B. Green. Modeling cyclic variability in spark-assisted HCCI. *Journal of Engineering for Gas Turbines and Power*, 130(5):052801, 2008.

[11] M. Havstad, S. Aceves, M. McNenly, W. Piggott, D. Edwards, R. Wagner, C. Daw, and C. Finney. Detailed chemical kinetic modeling of iso-octane SI-HCCI transition. In *SAE World Congress*, 2010. 10PFL-0840.

[12] B Zigler, P Keros, K Helleberg, M Fatouraie, D Assanis, and M Wooldridge. An experimental investigation of the sensitivity of the ignition and combustion properties of a single-cylinder research engine to spark-assisted HCCI. *Int. J. of Eng. Res.*, 12(4):353–375, 2011.

[13] R.P. Fitzgerald, R. Steeper, J. Snyder, R. Hanson, and R. Hessel. Determination of cycle temperature and residual gas fraction for HCCI negative valve overlap operation. *SAE Int. J. Engines*, 3(2010-01-0343):124–141, April 2010.

[14] E.A. Ortiz-Soto, J. Vavra, and A. Babajimopoulos. Assessment of residual mass estimation methods for cylinder pressure heat release analysis of HCCI engines with negative valve overlap. 2011. Accepted to ASME ICEF Tech. Conf., 2011.

[15] H.J. Yun and W. Mirsky. Schlieren-streak measurements of instantaneous exhaust gas velocities from a spark-ignition engine. *SAE*, (741015), 1974.

[16] John Heywood. *Internal Combustion Engine Fundamentals*. McGraw-Hill Science/Engineering/Math, 1988.

[17] M. Mladek and C. Onder. A model for the estimation of inducted air mass and the residual gas fraction using cylinder pressure measuremnts. *SAE International*, (23000-01-0958), 2000.

[18] F. Ponti, Piani J.C., and R. Suglia. Residual gas model for on-line estimation for inlet and exhaust continuous vvt engine configuration. *IFAC*.

[19] A. Gazis, D. Panousakis, J. Patterson, H.W. Chen, R. Chen, and J. Turner. Using in-cylinder gas internal energy balance to calibrate cylinder pressure data and estimate residual gas amount in gasoline homogeneous charge compression ignition combustion. *Experimental Heat Transfer*, 21(4):275–280, 2008.

[20] N. Ivansson. Estimation of the residual gas fraction in an HCCI engine using cylinder pressure. Master's thesis, Linköping Univ., May 2003.

[21] J. Chang, O. Güralp, Z. Filipi, D. Assanis, T.W. Kuo, P. Najt, and R. Rask. New heat transfer correlation for an HCCI engine derived from measurements of instantaneous surface heat flux. *SAE*, 1(2004-01-2996):1–18, 2004.

[22] E.Hellstroöm, J. Larimore, A. G. Stefanopoulou, J. Sterniak, and L.Jiang. Quantifying cyclic variability in a multi-cylinder HCCI engine with high residuals. In *ASME Internal Combustion Engine Division Spring Technical Conference*, 2012. ICES2012-81107.

[23] Y. Mo. *HCCI heat release rate and combustion efficiency: A coupled KIVA multi-zone modeling study*. PhD thesis, Univ. of Mich., 2008.

[24] Maximizing power output in an automotive scale multi-cylinder homogeneous charge compression ignition (HCCI) engine. In *SAE World Congr.*, 2011. SAE 2011-01-0907.

[25] S.H. Strogatz. *Nonlinear Dynamics and Chaos*. Perseus Books Publishing, LLC, 1994.